Computational Modeling of the Outflow of a Deep-Sea-Mining Collector-Vehicle

A Study of Numerical Fluid Mechanics Solution Methods

Christos Kakoutas

Department of Mechanical Engineering
Massachusetts Institute of Technology

Class 2.29: Numerical Fluid Mechanics

Final Project Presentation

Spring 2020

Outline

Research Area

Getting the Manganese Nodules from the Sea-Bed to the Sea-Surface

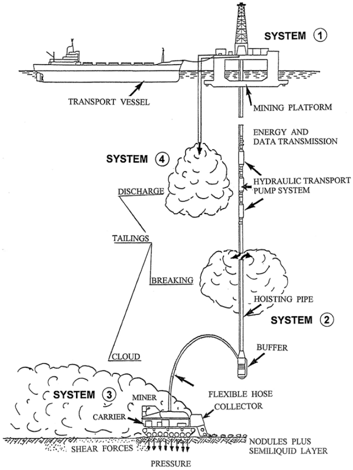

Figure 1: The overall mineral-extraction process [?].

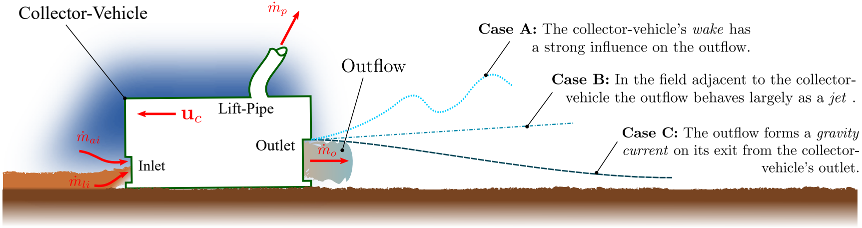

Figure 2: Different possibilities of the form which the outflow in the flow-field adjacent to the collector-vehicle can have.

Research Area

Dimensional Analysis Variables

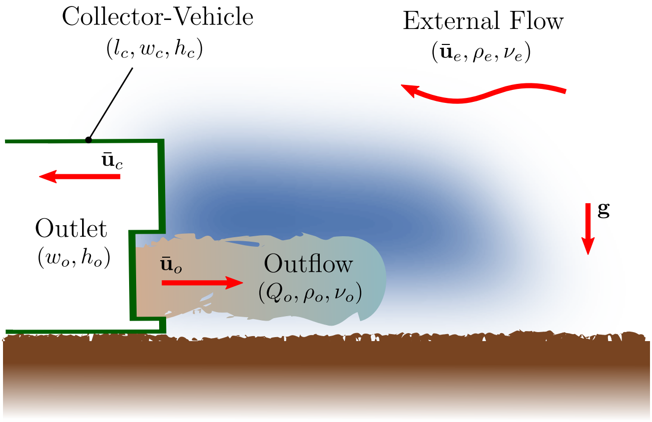

Figure 3: Introducing the variables and parameters relevant to our problem.

Table 1: Average Operating Conditions

(a) Flow Parameters

T $[C^o]$	ρ_e $[kgm^{-3}]$	μ_e $[kgm^{-1}s^{-1}]$	ν_e $[m^2s^{-1}]$
2	1.028×10^3	1.783×10^{-3}	1.734×10^{-6}

(b) Sediment and Outflow Properties

ρ_s $[kgm^{-3}]$	f_{so} $[-]$	ρ_o $[kgm^{-3}]$	μ_o $[kgm^{-1}s^{-1}]$	ν_o $[m^2s^{-1}]$
2.560×10^3	1.218×10^{-2}	1.047×10^3	1.838×10^{-3}	1.756×10^{-6}

(c) Collector-Vehicle Parameters

u_c $[ms^{-1}]$	h_c $[m]$	Q_o $[m^3s^{-1}]$
5.0×10^{-1}	5.0	1.5

Personal Objectives

Learnings to be materialised within the 2.29 Final Project

- Setting up a computational stencil which can capture the flow accurately.
- Learning how to create a mesh, coarsening and refining.
- Learning how to implement boundary conditions.
- Ensuring stability, accuracy and precision of the implemented scheme.
- Implementing a solution method ignoring multi-phase flow $\left(\frac{\nu_o}{\nu_e} = 1\right)$ to start with.
- Performing temporally short simulations at conditions $\left(Re_o, Re_c, Re_e \;\&\; \frac{\nu_o}{\nu_e}\right)$ less computationally demanding than true conditions.
- Compare Direct Numerical Simulations (DNS) against a Turbulence Model.

Personal Objectives

Tasks to be achieved for research purposes

- Implementing a solution method for multi-phase flows.
- Performing simulations at conditions $\left(Re_o, Re_c, Re_e \;\&\; \frac{\nu_o}{\nu_e}\right)$ represenative of true conditions.
- Expanding to a three-dimensional domain for flow calculation.

Mass Calculation:

$$\rho = f_o \rho_o + f_e \rho_e \quad ; \quad f_o + f_e \equiv 1 \quad \Longrightarrow \quad \rho = f_o(\rho_o - \rho_e) + \rho_e$$

Momentum Equation:

$$\underbrace{\frac{\partial(\rho \mathbf{u})}{\partial t} + \nabla \cdot (\rho \mathbf{u}\mathbf{u}) - \underbrace{\nabla \cdot \left[\mu \left(\nabla \mathbf{u} + \nabla \mathbf{u}^T\right)\right]}_{\text{modelled source term}}}_{\text{implicit}} = \underbrace{\underbrace{-\nabla(p)}_{\text{finite-volume surface-normal gradient scheme}}}_{\text{explicit; PIMPLE momentum predictor}}$$

PIMPLE Algorithm:

- SIMPLE (Semi-Implicit Method for Pressure-Linked Equations; suitable for steady-state problems) algorithm is implimented at every time step for the inner iterations
- PISO (Pressure Implicit with Splitting of Operator; suitable for transient problems) algorithm is implimented for the outer iterations.

Better stability is obtained from PIMPLE over PISO, especially when dealing with large time steps where the maximum Courant number may consistently be above 1, or when the nature of the solution is inherently unstable.

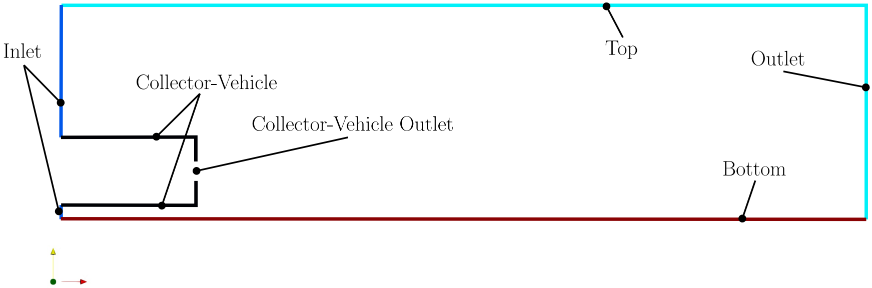

Figure 4: Mesh Boundaries.

Numerical Schemes

Parametric Investigation

Base-Case: $\frac{d}{dt}()_{Euler\ Implicit}$ $\nabla()_{Gauss\ Linear}$ $\nabla \cdot ()_{Gauss\ Linear\ Bounded}$ $\nabla^2()_{Gauss\ Linear\ Corrected}$ $Interpolation_{Linear}$

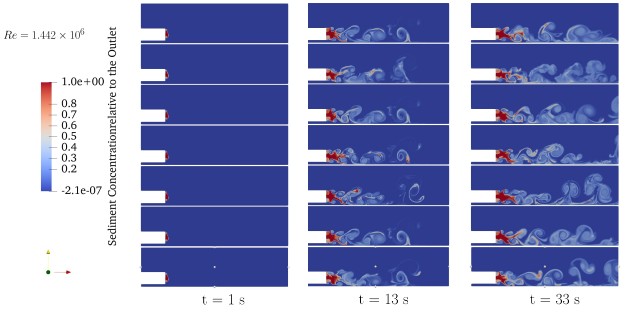

Changes:	Execution Time:
None	$610\ s\|_{t=33\ s}$
$\frac{d}{dt}()_{Crank-Nicolson}$	$754\ s\|_{t=33\ s}$
$\nabla()_{Gauss\ Cubic}$	$825\ s\|_{t=33\ s}$
$\nabla \cdot ()_{Gauss\ Linear}$	$578\ s\|_{t=33\ s}$
$\nabla \cdot ()_{Gauss\ Cubic}$	$1,007\ s\|_{t=33\ s}$
$\nabla^2()_{Gauss\ Cubic}$	$752\ s\|_{t=33\ s}$
$Interpolation_{Cubic}$	$965\ s\|_{t=33\ s}$

Figure 5: Impact of different Numerical Schemes on Stirring and Mixing

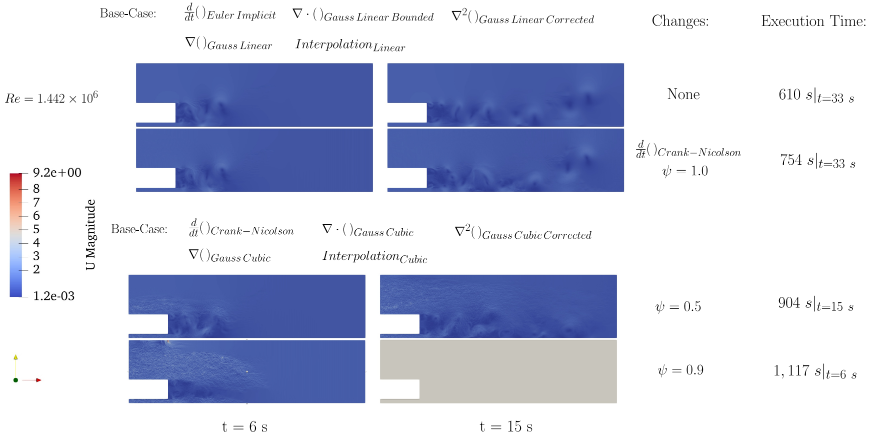

Figure 6: Differences in the calculated Velocity Field for different combinations of Euler Implicit and Crank-Nicolson schemes for the temporal derivatives.

Table 3: Parametric Study of Matrix-Problem Solvers

Scenario	tLMF_5	tLMF_12	tLMF_13	tLMF_14
Solver	twoLiquidMixingFoam			
CFL_{max}	0.5			
Cells	85536			
Uniform Grid	Yes			
Re [-]	1.442×10^6			
$[f_o]_{solver}$	Gauss-Seidel	PCG FDIC	Gauss-Seidel	
$[p]_{solver}$	GAMG relTol=0.01		PCG FDIC relTol=0.00	PCG FDIC relTol=0.01
$[\mathbf{u}]_{solver}$	Gauss-Seidel relTol=0.1			
Execution time [s]	6.099×10^2	6.304×10^2	2.174×10^3	1.333×10^3

Table 4: Parametric Study of Matrix-Problem Solvers

Scenario	tLMF_5	tLMF_15	tLMF_16
Solver	twoLiquidMixingFoam		
CFL_{max}	0.5		
Cells	85536		
Uniform Grid	Yes		
Re [-]	1.442×10^6		
$[f_o]_{solver}$	Gauss-Seidel		
$[p]_{solver}$	GAMG relTol=0.01	PCG diagonal relTol=0.01	GAMG relTol=0.01
$[\mathbf{u}]_{solver}$	Gauss-Seidel relTol=0.1		PBiCG diagonal relTol=0.1
Execution time [s]	6.099×10^2	1.923×10^3	1.130×10^3

Table 5: Parametric Study of Matrix-Problem Solvers

Scenario	tLMF_5	tLMF_17	tLMF_18	tLMF_19
Solver	twoLiquidMixingFoam			
CFL_{max}	0.5			
Cells	85536			
Uniform Grid	Yes			
Re [-]	1.442×10^6			
$[f_o]_{solver}$	Gauss-Seidel	GAMG	Gauss-Seidel	
Tolerance	10^{-9}			
Relative Tolerance	0.00			
$[p]_{solver}$	GAMG			Gauss-Seidel
Tolerance	10^{-7}			
Relative Tolerance	0.01			
$[\mathbf{u}]_{solver}$	Gauss-Seidel		GAMG	Gauss-Seidel
Tolerance	10^{-7}			
Relative Tolerance	0.10			
Execution time [s]	6.099×10^2	6.190×10^2	1.192×10^3	maximum iteration number

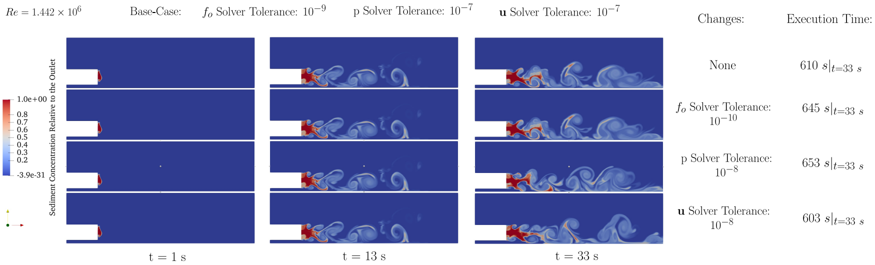

Figure 7: Impact of different Tolerances in implementing Matrix-Problem Solvers

Finalised Solution Method

Numerical Schemes and Matrix-Problem Solvers Combination

Table 6: Solution Method Components

(a) Numerical Schemes

$\frac{d}{dt}()$	$\nabla()$	$\nabla \cdot ()$	$\nabla^2()$	Interpolation
Euler Implicit	Gauss Linear		Gauss Linear Corrected	Linear

(b) Matrix-Problem Solvers

	f_0	p	**u**
Solver	Gauss-Seidel	GAMG Gauss-Seidel	Gauss-Seidel
Tolerance	10^{-9}	10^{-7}	10^{-7}
Relative Tolerance	0.00	0.01	0.10

Finalised Solution Method

Running on Parallel Processors

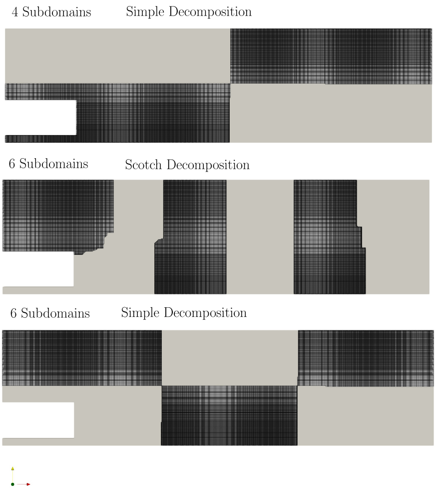

Figure 8: Domain Decomposition for running on Four and Six Parallel Processors.

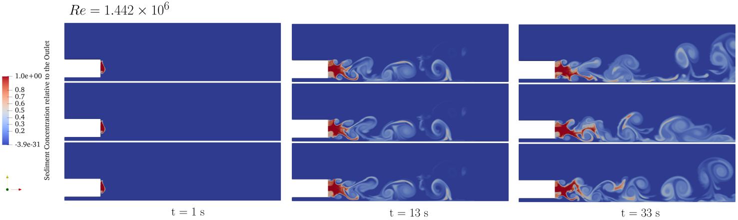

Number of Processors:	Execution Time:
1	$1,473\ s\|_{t=33\ s}$
4	$610\ s\|_{t=33\ s}$
6	$553\ s\|_{t=33\ s}$

Figure 9: Visual differences caused by parallel processing of the solution.

Physically Relevant Length-Scales

Resolution of Boundary Layers

$$\frac{\delta}{x} = 0.367 Re_x^{-1/5} \quad , \quad Re_x \equiv \frac{Ux}{\nu}$$

$$x \simeq 2\ m \quad \& \quad U \simeq 1\ ms^{-1}|_{\nu=1.734\times10^{-6}\ m^2 s^{-1}} \quad \Longrightarrow \quad \delta \simeq 2\ cm$$

This needs a mesh-density greater than 50 cells per meter.

Physically Relevant Length-Scales

Resolution of the Kolmogorov Microscale η_κ

$$\eta_\kappa \equiv \left(\frac{\nu^3}{\epsilon}\right)^{1/4} \quad , \quad \epsilon \simeq \frac{u^3}{L_t} \quad \Longrightarrow \quad \eta_\kappa \simeq L_t Re_t^{-3/4} \quad , \quad Re_t = \frac{uL_t}{\nu}$$

$$L_t \sim h_c = 2 = 1\ m \quad \& \quad u \sim u_c = 1\ ms^{-1}|_{\nu=1.734\times10^{-6}\ m^2s^{-1}}$$

$$\Longrightarrow \quad \eta_\kappa \simeq 50\ \mu m$$

This needs a mesh-density of the order of 21,000 cells per meter or greater.

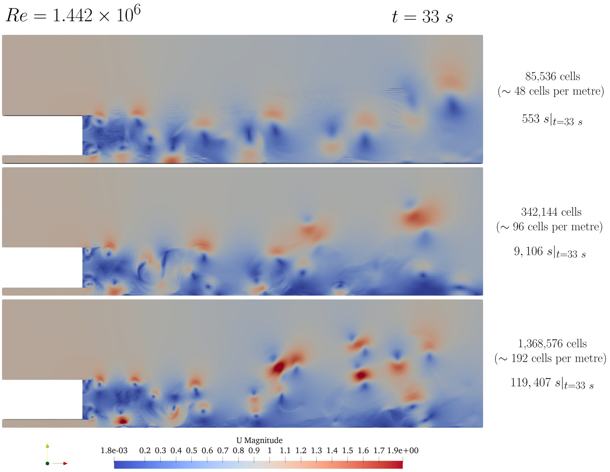

Figure 10: The effect of a progressively refined grid on the velocity field.

Physically Relevant Length-Scales

Changing the Reynolds Number

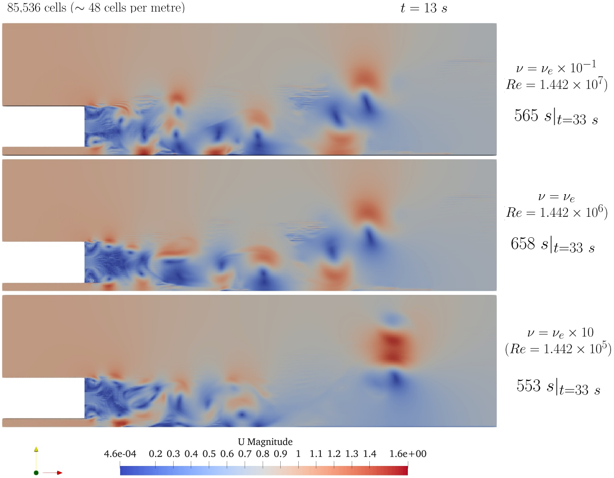

Figure 11: Effect of changing the Reynolds number on Numerical Artifacts.

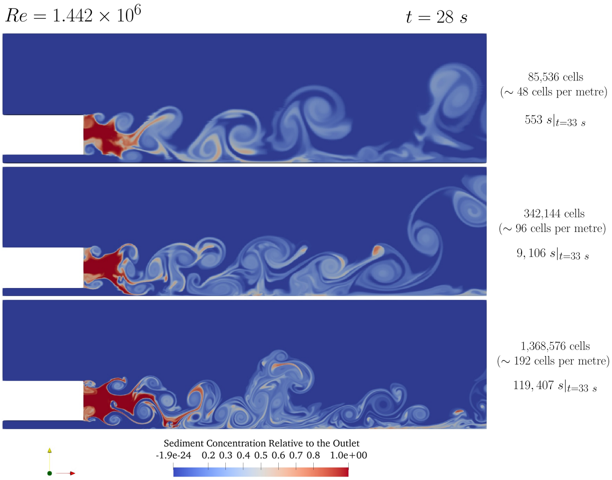

Figure 12: The effect of a progressively refined grid on Numerical Diffusion.

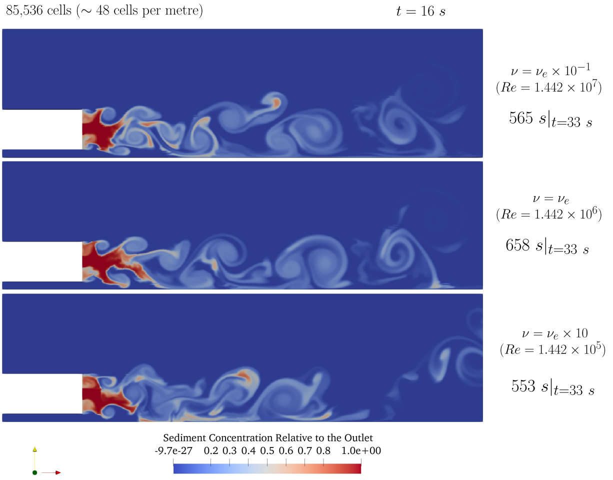

Figure 13: Comparing Fluid Viscosity with Numerical Diffusion.

Concluding Remarks

Main Learnings

- Stability is determined by the nature of the governing equations and the boundary conditions.
- Stability influences the choice of numerical schemes, the order of accuracy, and the need for boundedness.
- The truncation error in the divergence operator is the most significant contributor for numerical diffusion, when the numerical schemes of the same order of accuracy are used for all operators.
- Energy conserving numerical schemes such as Crank-Nicolson capture turbulence effects relatively well even for unresolved computational grids.
- In order to get a physically right solution the grid needs to be resolved, or transport properties need to be modelled accordingly.
- Given the grid is resolved, the matrix-problem solvers will give an accurate solution. The solution will be precise if the tolerance of the solvers is set accordingly.
- The type of matrix-solver to be used depends on the stability of the problem, the field-variables solved for, and the solution algorithm implemented.

- For the volume-of-fluid method implemented for the mixing of two miscible fluids using the PIMPLE algorithm, Gauss-Seidel smooth solvers for volume-fraction and velocity and GAMG solver for pressure seem to perform better in terms of accuracy and computational cost than alternatives.
- The problem is very sensitive to boundary conditions, and for unresolved grids oscillatory discretisation schemes such as Crank-Nicolson lead to instability.
- The solution was not physically correct for grids too coarse to resolve the Kolmogorov turbulence microscale.

Bibliography I

OpenFOAM The Open Source CFD Toolbox User Guide, 2019.

Christopher J. Greenshields.
OpenFOAM User Guide, 2019.

GSR.
Environmental impact statement.
Environmental Impact Statement, 18(1), 2000.

ITTC.
Recommended Procedures and Guidelines - Fresh Water and Seawater Properties - 7.5-02-01-03.
International Towing Tank Conference, (7.5-02-01-03), 2011.

Bibliography II

Kenneth Moreland, Utkarsh Ayachit, Berk Geveci, Cory Quammen, Dave Demarle, Kenneth Moreland, Andy Bauer, Ben Boeckel, Dan Lipsa, Mathieu Westphal, Joachim Pouderoux, Shawn Waldon, Aashish Choudhary, Sujin Philip, George Zagaris, Burlen Loring, Thomas Maxwell, John Patchett, James Ahrens, Boonthanome Nouanesengsy, and Bill Sherman.
The ParaView Guide.
Sandia National Laboratories, page 251, 2016.

Horst U. Oebius, Hermann J. Becker, Susanne Rolinski, and Jacek A. Jankowski.
Parametrization and evaluation of marine environmental impacts produced by deep-sea manganese nodule mining.
Deep-Sea Research Part II: Topical Studies in Oceanography, 48(17-18):3453–3467, 2001.

Bibliography III

Zhongfan Zhu, Hongrui Wang, and Dingzhi Peng.
Dependence of sediment suspension viscosity on solid concentration: A simple general equation.
Water (Switzerland), 9(7), 2017.